Chapter 5

Asymmetry of extensive air showers at ground level

5.1 Introduction

The LDD of shower particles in an EAS in the shower front plane is assumed to be symmetric about the shower axis and the corresponding LDF is also symmetric. Due to stochastic nature of their developments in the atmosphere, these axial symmetries are affected differently from one shower to other. For a vertically incident shower, the shower front plane more or less coincides with the observed plane and the equi-density zones in the LDD are circles in the observed plane. Hence, the LDF that describes the LDD of EAS particles for vertical showers must be polar symmetric, while for inclined EASs some sort of polar averaged densities would be appropriate. For nearly inclined showers with $\Theta \geq 18^0$, the equi-density zones are approximated to ellipses [1–3]. This structure of LDD arises from the attenuation of polar densities due to unequal traversal of paths by EAS particles at different polar positions around the shower axis in the observed plane. Therefore, employment of the circular symmetry to density data in inclined showers may lead to systematic errors in estimating various EAS parameters including the core. Distortion in LDD also arises from the geomagnetic effect on charge particles in an EAS but such an effect is noticeable on the muon component for highly inclined showers with $\Theta > 60^0$ [4].

For non-vertical showers, the asymmetry in the LDD of EAS particles is described as an elongation of equi-density circles to ellipses. The center of these

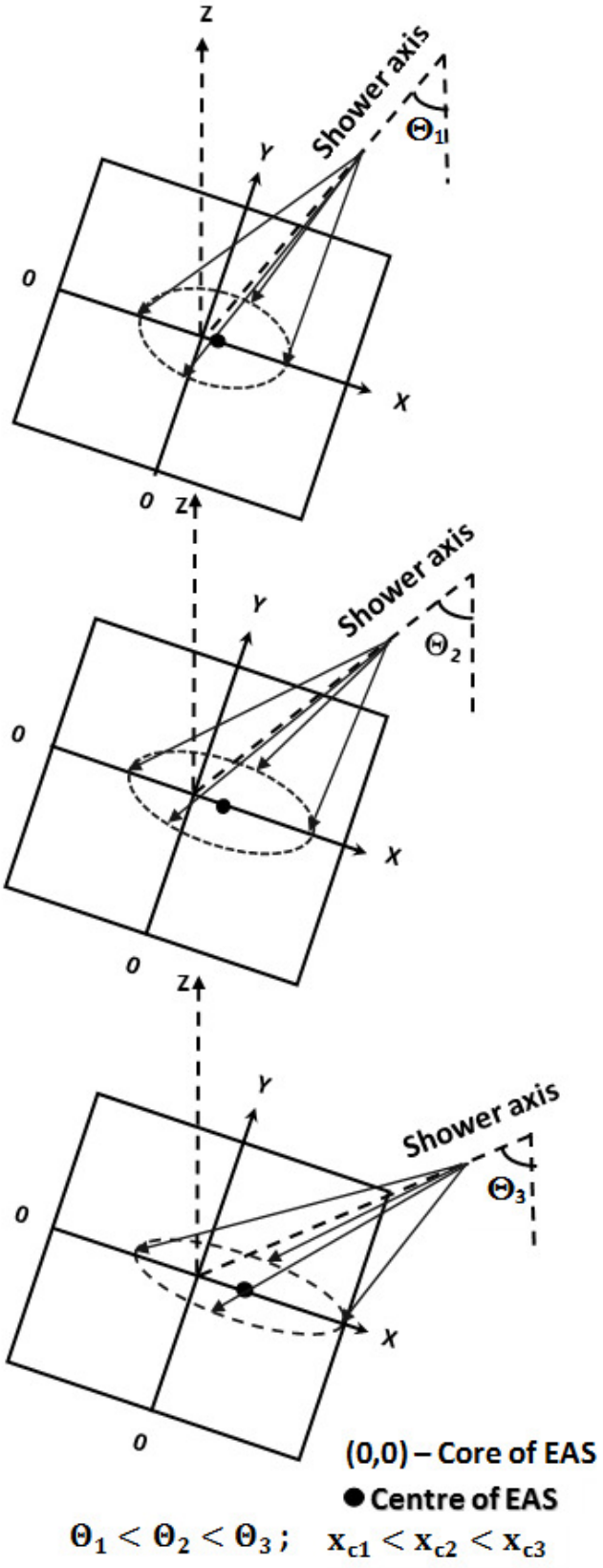

FIGURE 5.1: Structure of equi-density ellipses in three different angles of incidence and the corresponding variation of the gap length between the EAS core and the center of the equi-density ellipse.

annular equi-density ellipses do not overlap with the EAS core. The so-called gap length (GL) between the center of equi-density ellipses and the EAS core will be developed, whose magnitude may determine the attenuation power of different types of EAS particles in the atmosphere for a given incidence. A clear picture of such a situation is viewed in the Fig. 5.1 with increasing zenith angle of the EAS.

For the reconstruction of LDD of shower particles of an observed non-vertical shower, a modified or elliptic-LDF (ELDF) should be used instead of a polar symmetric-LDF (SLDF) in the ground-plane. If the GL defined above is included in the LDF, then more precise EAS parameters can be obtained from the analysis of data. To extract actual variation introduced by the attenuation effects to the EAS observables, as a first step, it is necessary to take away the contribution added geometrically from density data. A projection of polar density from the ground plane to the shower front plane can be implemented through two ways. In the first case, without any GL, when the EAS particles are assumed to suffer no interaction in the space between the shower front plane and the ground plane. Secondly, to introduce the atmospheric attenuation of shower particles to the LDF, the projection including the GL should be taken into account during the formulation of the ELDF. Using MC data, we have validated the consideration of the ELDF for the elliptic LDD in Sec. 5.5.

This work is mainly aimed to structure analytically the asymmetric LDD of the EM component of an EAS that involves the GL. In doing so, we have to look for the existence of the gap using simulated data obtained from MC generated showers with different primary energies and zenith angles. The formation of the GL due to attenuation of EAS in the atmosphere will be formulated. Results obtained from the modified analytical function for the LDF indicate how the GL varies with the zenith angle, and core distance. Moreover, an analytical representation of the ELDF including the gap will be made from a polar SLDF without any gap. Dependence of the GL parameter on some commonly used EAS observables will be studied for exploring some signature of discriminating light and heavy primaries. The radial variation of the shower age parameter of an EAS [5–7] using ELDF and SLDF will also be investigated.

The present chapter consists of several sections as follows. In the next section

5.2, we model the GL arises from the atmospheric attenuation of the EM component of EAS using a most common longitudinal profile (cylindrical type) of the EAS development. A complete formulation of the polar ELDF from the modeling of the GL in the selected cylindrical profile will be described in the section 5.3. In the same Sec., an appropriate formula for the LAP will be given using the ELDF. In section 5.4, we report important features of the MC simulation used in our analysis. Our results using simulated showers and their comparisons with the model dependent calculations on several aspects of attenuation effect are discussed in the section 5.5. Potentiality of identifying the nature of EAS initiating particle by the GL parameter is also included. Implementation of the new ELDF to simulated data for re-examining the radial dependence of the shower age parameter and hence its primary mass sensitivity are also presented in section 5.5. In section 5.6, a brief discussion on the entire work is presented. Finally, our conclusions are given in section 5.7.

5.2 The cylindrical EAS profile

Indication of the atmospheric attenuation in vertical showers is hardly noticed, while for inclined showers such effect alters the center of concentric equi-density ellipses. The position of the modified center for inclined showers compared to vertical showers will depend upon the amended longitudinal profile in the atmosphere. Most common longitudinal EAS profile is the cylindrical one, in which all the EAS particles advance downward parallel to the EAS core in the front plane. In this profile, equi-density zones for vertical showers are expected to be circles in both ground and shower front planes. In Fig. 5.2, we have depicted the profile for an inclined EAS that hits the ground surface arriving from the North direction (i.e. azimuthal angle, $\Phi = 0^0$). The geometric correction is done through the projection of the ground plane (elliptic) to a circle which is normal to the EAS axis.

A cosmic ray (CR) shower advances like a circular front plane towards the ground from the North (here), it intersects the ground plane across Y-axis (see Fig. 5.2), when the EAS core just hits the origin of the coordinate system under consideration. According to the cylindrical profile of the EAS development, if a secondary particle hits the front plane at a point A (x_s, y_s), then its corresponding point on

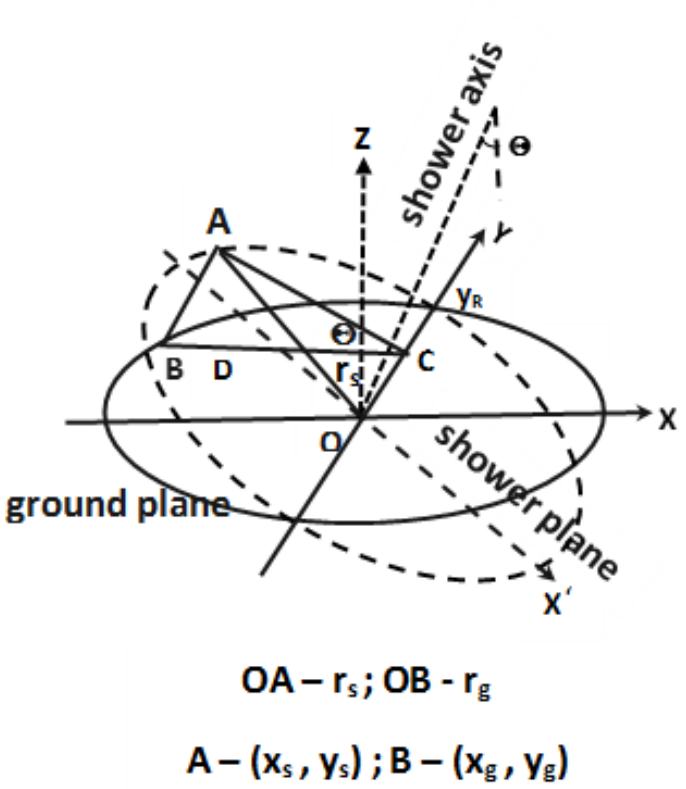

FIGURE 5.2: Sketch of the geometry of the ground plane and shower front plane of an inclined shower.

the ground plane be at B (x_g, y_g). Let r_s denotes the radius of the circle containing the point A (i.e. $OA = r_s$ in the shower plane). The distance of the point A as well as B in the Y-direction is given by the element OC. From the geometry, it is easy to show that lengths AC and BC make an angle which is actually the zenith angle (Θ) of the EAS. Now, we can relate all these line elements when B, being a projection of A in the ground plane, to obtain the following connections,

$$AC^2 = r_s^2 - y_g^2, r_s^2 = x_g^2 cos^2\Theta + y_g^2, AB^2 = x_g^2 sin^2\Theta. \tag{5.1}$$

It is easier to relate particle density at the ground plane, $\rho_g(r_g \equiv x_g, y_g)$ with the same at the front plane, $\rho_s(r_s)$ when the EAS particles do not suffer any loss due to attenuation and it is given by [8],

$$\rho_s(r_s) = \frac{\rho_g(r_g)}{cos\Theta}. \tag{5.2}$$

Without any attenuation in the space between the ground and shower front planes, it is clear from the Fig. 5.2, that the observed and shower planes intersect each other at a distance y_R along the Y-axis due to geometric correction only. Therefore, introducing y_R, we have the following equation that works in the ground plane,

$$x_g^2 cos^2\Theta + y_g^2 = y_R^2. \tag{5.3}$$

As described in the model that the attenuation effect causes a linear translation of the center of the ellipse from the EAS core. This will be verified using MC data and given in the Sec. 5.5. If such a translation of the center along the X-axis in the ground plane is denoted by x_C, then equation 5.3 takes the following form

$$(x_g - x_C)^2 cos^2\Theta + y_g^2 = b^2, \tag{5.4}$$

where b measures the length of semi-minor axis for the new ellipse. For $x_g = 0$ in the equation 5.4, y_g takes its old value y_R and we get,

$$x_C^2 cos^2\Theta + y_R^2 = b^2. \tag{5.5}$$

Inserting equation 5.5 in 5.4, we will get the required equation for the modified ellipse which is given by

$$x_g^2 - 2x_g x_C cos^2\Theta + y_g^2 = y_R^2. \tag{5.6}$$

An appropriate analytical expression for the ELDF can be obtained from the solution of the above equation.

5.3 Modeling the effect of attenuation on the polar density of EAS

5.3.1 Analytical approach for the determination of the linear gap

The total charge particle content (comprising more than $\sim 99\%$ by electrons and muons) of an EAS follows roughly an exponential fall after reaching its maximum size. Similarly, the LDD of EAS particles for any particular type of secondaries has found to decrease exponentially with the core distance for both the observed as well as MC data. Different groups implemented different LDFs for describing the LDD depending upon various factors, like primary energy, type of EAS particles, altitude etc. But in those LDFs, probably attenuation contribution of shower particles in the space between the ground and shower front planes was not considered. Keeping all these earlier efforts in mind, one may therefore introduce a *characteristic function* (CF) for the LDD, to describe approximately its exponential behavior with r_s. Hence, under the circumstance we can describe the LDD roughly by the following function,

$$\rho(r_s) \simeq c.e^{-\alpha(\frac{r_s}{r_0})^{\kappa}}, \tag{5.7}$$

where α and κ are some dimensionless parameters, and c, being a constant expressed in m^{-2}. These constants can be obtained from the fitting of polar lateral density of the EM component, and r_0 is some characteristic unit of length in the interaction process.

An EAS is in its attenuation phase when the depth of the shower exceeds the depth of shower maximum ($X_{\max}$) [9]. Attenuation effects in the space between A and B reduces the density of EAS particles which is of course very marginal, but would follow an exponential fall by a factor $e^{-(X-X_g)/\Lambda}$. Here, $X - X_g = \Delta X$ g cm^{-2} measures the extra path traversed by EAS particles from A to B and Λ, the attenuation length in g cm^{-2}. From [8], we have the attenuated density ρ_g of a particular kind of EAS particles in the ground in terms of Λ, Θ and ρ_s, which is given by

$$\rho_g(r_g) = cos\Theta.\rho_s(r_s).e^{-\frac{\Delta X}{\Lambda}}. \tag{5.8}$$

By simple unit conversion into linear scale, the equation 5.8 reduces to the form as follows,

$$\rho_g(r_g) = cos\Theta.\rho_s.(r)e^{-\eta.AB}, \tag{5.9}$$

where η is the attenuation length in the unit of the reciprocal of linear distance. From the geometry of the cylindrical EAS profile, we have to substitute $\pm x_g sin\Theta$ (-ve sign is taken corresponding to the attenuation of the late part of the EAS) for the additional path AB in the equation 5.9, it then becomes

$$\rho_g(r_g) = cos\Theta.\rho_s(r_s).e^{\eta x_g sin\Theta}. \tag{5.10}$$

The attenuation effect on inclined EASs will give rise a modification of the center of elliptic density zones in the ground plane and thereby giving a more reliable estimation for the polar density including the new center of equi-density ellipses. Putting $x_g = 0$ in equation 5.3, we get $y_g = y_R$, then equation 5.10 becomes

$$\rho_g(r_g)_{x_g=0,y_g=y_R} = cos\Theta.\rho_s(y_R). \tag{5.11}$$

Density of particles in an elliptic contour in the ground plane corresponding to $y = y_R$, for example, does not depend on x_g which means, $\rho_g(x_g, y_g) = \rho_g(0, y_R)$ and hence $\rho_g(x_g, y_g) = cos\Theta.\rho_s(y_R)$. This suggests that the equation 5.11 will get the following form,

$$\rho_g(r_g or(x_g, y_g)) = cos\Theta.\rho_s(y_R). \tag{5.12}$$

By inserting the equation 5.12 into 5.10, we obtain one of the important equations dealing attenuation effects on shower particle density, which is given by,

$$\rho_n(y_R) = e^{\eta x_g sin\Theta}.\rho_s(r_s). \tag{5.13}$$

We have already introduced the CF for the LDD, the above equation can be written now as,

$$e^{-\alpha(\frac{y_R}{r_0})^\kappa} = e^{\eta x_g sin\Theta}.e^{-\alpha(\frac{r_s}{r_0})^\kappa}. \tag{5.14}$$

After simplification, we have obtained the following,

$$r_s^2 = y_R^2(1 + \frac{\eta x_g sin\Theta}{\alpha(\frac{y_R}{r_0})^\kappa})^{\frac{2}{\kappa}}. \tag{5.15}$$

If we introduce $\delta = \frac{\eta tan\Theta}{\alpha\kappa(\frac{y_R}{r_0})^\kappa}$ in the above equation 5.15, and then it can be rewritten as

$$r_s^2 = y_R^2(1 + x_g\kappa\delta cos\Theta)^{\frac{2}{\kappa}}. \tag{5.16}$$

Since the product $x_g\kappa\delta cos\Theta$ is much smaller than 1 for conventional EAS arrays like KASCADE [10], GRAPES-3 [11] etc. (e.g. x_g will be within 500 m in GRAPES-3 even after proposed expansion of the array) and one may therefore write an approximate form of the above relation 5.16 into

$$r_s^2 \approx y_R^2(1 + 2x_g\delta cos\Theta). \tag{5.17}$$

Replacing r_s by the equation 5.1, we will get following equations after rearranging few terms,

$$(x_g cos\Theta - y_R^2\delta)^2 + y_g^2 \approx y_R^2(1 + y_R^2\delta^2) \tag{5.18}$$

$$(x_g - \frac{y_R^2\delta}{cos\Theta})^2 + y_g^2 sec^2\Theta = y_R^2 sec^2\Theta(1 + y_R^2\delta^2). \tag{5.19}$$

These equations when compared with the equation 5.4, the model predicted shift of the center of equi-density ellipses along the X-axis in the ground plane takes the following form:

$$x_C \cong \frac{y_R^2\delta}{cos\Theta}, \tag{5.20}$$

or,

$$x_C = y_R^{2-\kappa} r_0^\kappa . sin\Theta sec^2\Theta . \eta(\alpha\kappa)^{-1}. \tag{5.21}$$

For a given Θ and particular set of values for all the remaining quantities in the equation 5.21, the GL appears to be positive (i.e. $x_C > 0$). This suggests that the attenuation effect on the EAS according to the adopted model predicts a movement of the center of the equi-density ellipses into the early part of the EAS. The order of magnitude of the GL between the EAS core and the new center will be checked in the Sec. 5.5 using MC data.

5.3.2 The polar elliptic lateral density function (ELDF)

The relationship between x_C and Θ involving y_R, r_0, η, and dimensionless parameters (α, κ etc.) through the equation 5.21 plays a significant role to provide a well accepted parametrization for the ELDF in the ground plane. Let us recalling the equation 5.6, into which we will insert a more suitable form of the parameter x_C. Rewriting the expression for x_C to get its new form as follows

$$x_C = 2A_f y_R tan\Theta, \tag{5.22}$$

where, we have used the factor A_f for $\frac{r_0}{cos\Theta}\eta(\alpha\kappa)^{-1}$. Hence the equation 5.6 becomes

$$(x_g^2 - 4x_g.A_f y_R.tan\Theta)cos^2\Theta + y_g^2 = y_R^2, \tag{5.23}$$

$$y_R^2 + 4x_g.A_f y_R.tan\Theta cos^2\Theta + (x_g^2 cos^2\Theta + y_g^2) = 0. \tag{5.24}$$

We get the value for y_R after solving the above equation

$$y_R = -A_f x_g sin2\Theta + [y_g^2 + x_g^2(1 + 4A_f^2 sin^2\Theta)cos^2\Theta]^{\frac{1}{2}}, \tag{5.25}$$

$$y_R \approx -A_f x_g sin2\Theta + (y_g^2 + x_g^2 cos^2\Theta)^{\frac{1}{2}}. \tag{5.26}$$

We obtain the equation 5.26 from 5.25, if $A_f << 1$ and it will be verified later (Sec. 5.5). Introducing polar coordinates i.e. (r_g, β_g) in place of the cartesian set (x_g, y_g), the equation 5.26 can take the form

$$y_R = -A_f.r_g cos\beta_g.sin2\Theta + (r_s^2)^{\frac{1}{2}}, \tag{5.27}$$

Or,

$$y_R = -A_f.r_g cos\beta_g.sin2\Theta + r_g(1 - cos^2\beta_g sin^2\Theta)^{\frac{1}{2}}. \tag{5.28}$$

It is clear that the presence of the first term on the right hand side of equation 5.28 is due to the atmospheric attenuation effect, without the term, the expression for y_R looks similar as reported in [8]. The polar ELDF in the ground plane can be obtained by substituting the equation 5.28 in 5.12 for polar coordinates (replacing $\rho_g(x_g, y_g) \equiv \rho_g(r_g, \beta_g)$ and y_R by the above equation). Now, we have to look for a more judicious SLDF i.e. $\rho_s(y_R)$ after validation by the MC data in order to get ELDF, $\rho_g(r_g, \beta_g)$.

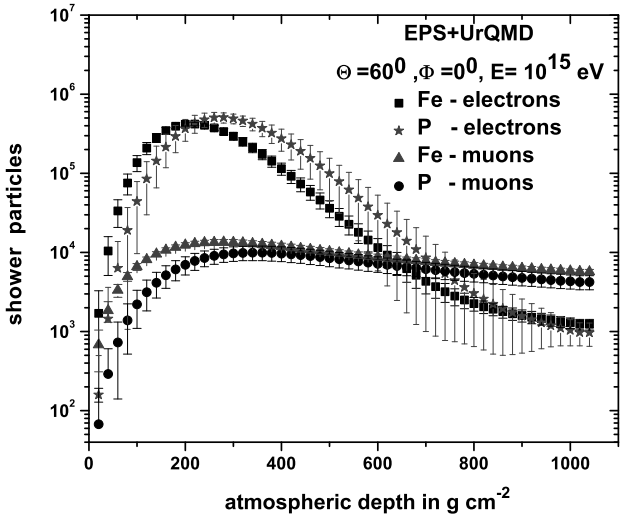

FIGURE 5.3: Longitudinal distribution of average electrons and muons for proton and iron induced showers at KASCADE level.

The analysis of arrival times of shower particles from timing measurements observed a difference in the average arrival times between the EM and muon components [12]. This actually corroborates the well-known fact that the EM component attenuate differently with respect to muons during the EAS development and hence they should follow different attenuation laws. We have checked it by studying the average development of electrons and muons for $\Theta = 60^0$ in the Fig. 5.3 to observe their attenuation power in the atmosphere. It is seen that the muon attenuation is negligibly small in the space between the ground and shower front planes. Consequent upon, we have considered only the EM component of an EAS for the present study. It is worth noting to state that while developing in the

atmosphere of an EAS, the perpendicular component of the geomagnetic field (GF) distorts trajectories of secondary charged particles. For that reason, the GF induces a polar modulation or asymmetry on densities of air shower particles. But the effect of GF on the EM component is less pronounced, in comparison with the attenuation effect on them [13]. Hence, for the improvement of the fitting quality to experimental data one should use the equation 5.10, which computes the ELDF with attenuation in the ground plane from a polar SLDF in the shower front plane. Application of that type of ELDF for the reconstruction of showers will lead to provide more accurate EAS observables including the shower core.

Over the period of time, many LDFs came into existence in air shower physics, used in various experiments [10] for the LDD of EAS electrons or total charged particles, the Nishimura-Kamata-Greisen (NKG) [14, 15] function is known to be the prime which actually gave away first by Greisen, is written as

$$\rho(r_s) = C(s_\perp) N_e . (r_s/r_0)^{s_\perp - 2} (1 + r_s/r_0)^{s_\perp - 4.5} \, , \tag{5.29}$$

where $C(s_\perp)$ is the normalization factor, while $s_\perp$, r_0 and N_e respectively are called the age parameter, the Moliére radius and shower size [14]. The polar ELDF can be found from the NKG type SLDF by making a substitution for the variable r_s by y_R in equation 5.29 and then apply it into the equation 5.12 after inserting the equation 5.28 for y_R again. Hence, the equation for the ELDF finally takes the following structure.

$$\rho(r_g, \beta_g) = cos\Theta . C(s_\perp) N_e . (y_R/r_0)^{s_\perp - 2} (1 + y_R/r_0)^{s_\perp - 4.5} \, , \tag{5.30}$$

with y_R according to the equation 5.28.

5.3.3 Modified local age parameter

The SLDF (actually the NKG-type LDF) in the equation 5.29 does not work if $s_\perp$ experiences a variation with core distance. This behavior was verified the AkenoAkeno, KASCADE and NBU experiments using observed electron density data [6, 16]. It otherwise suggests that $s_\perp$ becomes a variable of the core distance of an EAS. As a diagnosis to the problem an alternative approach was furnished

bestowing the concept of LAP [5]. This is eventually an estimation of shower age parameters at different arbitrary points from the EAS core. Moreover, we have already obtained a modified LDF like ELDF in place of NKG in this work, and it is expected that inclusion of it might also change the LAP and its radial variation. Assuming a pair of two adjacent positions, at $y_R(1)$ and $y_R(2)$, the LAP for the ELDF $\rho(X_R)$ with ($X_R = \frac{y_R}{r_0}$) in $[X_R(1), X_R(2)]$:

$$s_{LAP}(1,2) = \frac{\ln(F_R(12)X_R(12)^2Y_R(12)^{4.5})}{\ln(X_R(12)Y_R(12))} \tag{5.31}$$

Here, $F_R(12) = \rho(y_R(1))/\rho(y_R(2))$, $X_R(12) = y_R(1)/y_R(2)$, and $Y_R(12) = (X_R(1)+1)/(X_R(2)+1)$. When $y_R(1) \to y_R(2)$, it actually yields the LAP, and is $s_{LAP}(X_R)$ (or $s_{LAP}(r_g, \beta_g)$) at a position :

$$s_{LAP}(X_R) = \frac{1}{2X_R+1}\left((X_R+1)\frac{\partial \ln \rho}{\partial \ln X_R} + 6.5X_R + 2\right) \tag{5.32}$$

The density function $\rho(r_g, \beta_g)$ now involves $s_{LAP}(r_g, \beta_g)$ instead of single $s_\perp$ to fit $\rho(r_g, \beta_g)$ around an arbitrary point in the ground plane within aa elemental zone comprising Δr_g and $\Delta\beta_g$.

This representation of $s_{LAP}(r_g, \beta_g) \equiv s_{LAP}(1,2)$ for mean distance $y_R = \frac{y_R(1)+y_R(2)}{2}$ works nicely for MC data (with $F_R(12) = \rho(y_R(1))/\rho(y_R(2))$.

5.4 Simulation by the *CORSIKA* code

We have exploited the MC simulation code *CORSIKA* (**CO**smic **R**ay **SI**mulation for **KA**scade) of version 6.970 [17]. Simulated events are generated with high energy model EPOS 1.99 [18], and with low energy model UrQMD [19] for hadronic interactions. Interactions among EM components are made by the simulation program EGS4 [20] that can be treated as an important model for the cascade development involving electrons and photons. The flat atmospheric model [21] which is valid below the zenith angle 70^o, is considered for the work. The simulation is performed at the KASCADE condition only. Nearly 500 simulated showers are generated using proton and iron primaries at five primary energies

1, 5, 10, 100 and 1000 PeV respectively with the zenith angle 50^0 corresponding to energy cuts 0.5 GeV, 230 MeV, and 3 MeV for hadrons, muons and EM - part+photons. We have also generated a smaller sample of showers at each case of Θ: 55^0, 60^0, 65^0 and 69^0 for 100 PeV. For extracting the nature of EAS initiating primaries using the modified LAP, allowing fluctuations, about 500 more showers are also generated restricting Θ and E to some regions with $50^0 \leq \Theta \leq 60^0$ and $10 \leq E \leq 50$ PeV. We have used thinning option of *CORSIKA* for primary energies ≥ 100 PeV only by taking 10^{-6} as thinning factor according to the optimum weight limitation [22]. In our generated showers, we have restricted all showers with $\Phi = 0^o$ so that the EAS cores will always appear on the X-axis.

5.5 The analysis of Monte Carlo data and results

As discussed above, the present investigation applies only to electron density data for the purpose of shower reconstruction by the ELDF. For each shower, the simulated lateral electron densities are estimated in 180 mean angular positions around the EAS core with a step size of $\delta\beta_g = 2^0$ each in the ground plane. The successive radial step size within each angular bin increases by 1 m up to $r_g = 75$ m, 2 m up to $r_g = 150$ m, 3 m up to $r_g = 250$ m, and 5 m for 350 m and so on. From the output MC data file, β_g and r_g can be estimated with the help of x_g,y_g values for each electron in the ground plane.

In the Fig. 5.4, we compare the reconstructed polar electron densities obtained using SLDF, ELDF plus projection and ELDF plus both projection and attenuation at two core distances 50 and 75 m respectively for an average 5 PeV proton shower with $\Theta = 50^0$ coming from the North direction in the *CORSIKA* geometry. It is noted that the ELDF-(projection+attenuation) gives a higher angular variation of electron density compared to ELDF (only projection) or SLDF respectively. This result reconfirms that the ELDF with a GL is more appropriate for the reconstruction of non-vertical EASs. On the other hand, such polar variations are robust at larger core distances. In the top of the Fig. 5.4, the ratio between the maximum and minimum densities is $\frac{\rho_{r_g=50}(\beta_g=0^0)}{\rho_{r_g=50}(\beta_g=90^0)} = 3.03$, while in the bottom figure, it is $\frac{\rho_{r_g=75}(\beta_g=0^0)}{\rho_{r_g=75}(\beta_g=90^0)} = 3.46$.

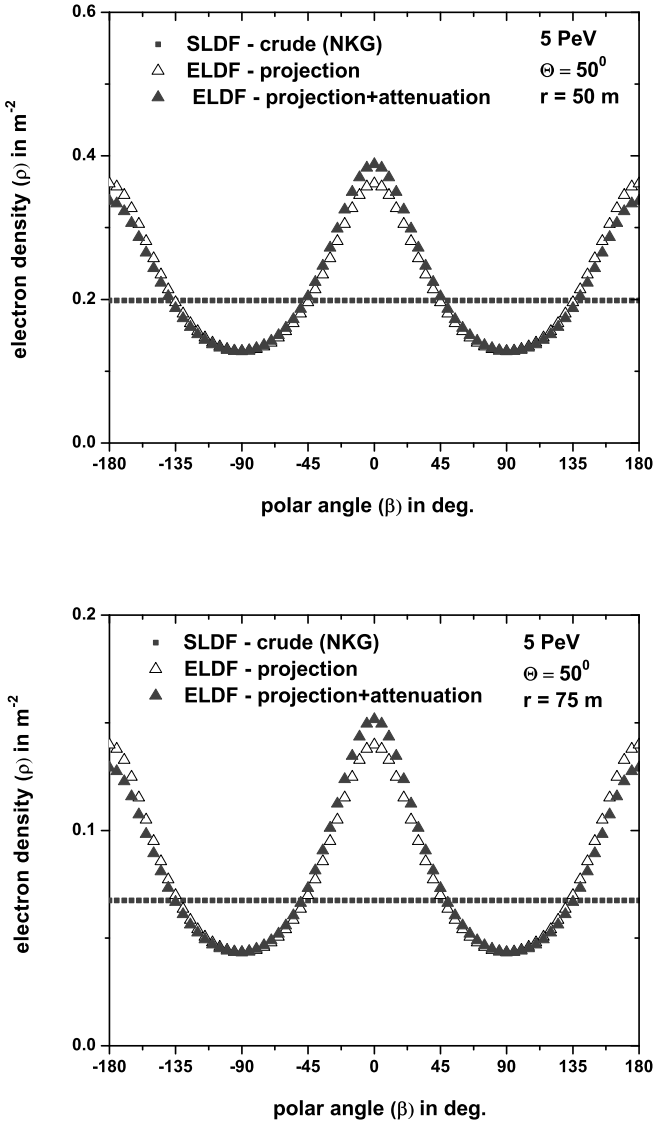

FIGURE 5.4: Polar distribution of electrons from the simulated data. Top: $r \equiv r_g = 50$ m, Bottom: $r \equiv r_g = 75$ m.

It has already been shown in Sec. 5.3 that the so called GL is obtained analytically by applying some approximate LDF (CF) for the lateral electron density. We have plotted average electron densities with core distance estimated at $\beta_g = 45^0$ averaging between polar angles 44^0 and 46^0 apart, for P and Fe initiated showers in the Fig. 5.5. These two lateral density curves are approximated by the CF corresponding to two nearly equal sets of parameters for α and κ. From the best possible fitting of the simulated data the parameter α picks values 3.43 and 3.52 while κ takes 0.5 and 0.47 respectively for P and Fe.

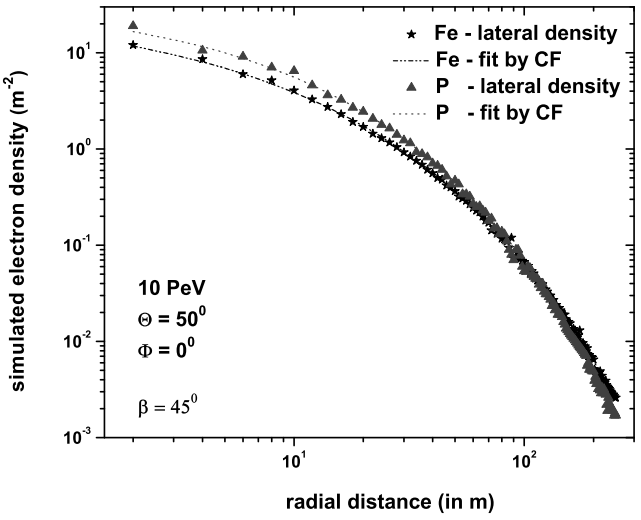

FIGURE 5.5: Electron lateral density from simulated data for proton and iron initiated showers in the ground plane. Density data are fitted by the characteristic function (CF).

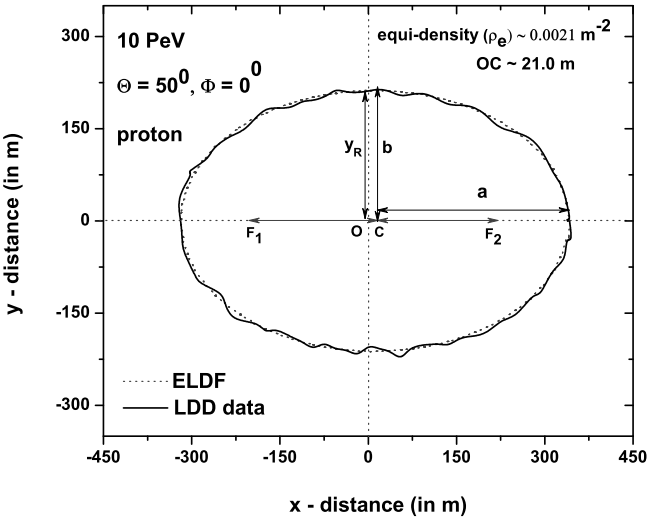

FIGURE 5.6: Formation of the GL from the equi-density ellipse of the simulated electron density.

5.5.1 The gap length from equi-density contour of polar LDD of electrons

In the beginning of the Sec. 5.5, the procedure of estimating the simulated electron densities and their reconstruction by the ELDF has been described. In Fig. 5.6, an equi-density ellipse for the electron density $\rho_g \sim 0.0021$ m^{-2} initiated by a 10 PeV proton shower is depicted in the horizontal $x_g - y_g$ plane. In our data analysis, we have different sets of (r_g, β_g) corresponding to the equi-density, ~ 0.0021 m^{-2}. Using transformations, $x_g = r_g cos\beta_g$ and $y_g = r_g sin\beta_g$, it can be shown with respect to the cartesian set of coordinates. The black solid line in the figure shows the equi-density zone obtained from the simulated data employing our scanning procedure used for estimating equi-density electron density data. The approximated equi-density ellipse is shown by the dotted line. The center of the equi-density ellipse experiences a translation from O to C due to the atmospheric attenuation of EAS electrons. From the figure, the GL comes out to be ~ 21.0 m from the approximated ellipse. We still have the elliptic LDD but with a displaced center, new focal points and modified lengths for the minor, and major axes.

The model predicted linear gap can be evaluated using the equation 5.21 for x_C as follows:

Here, we substitute our best fit values as obtained for α and κ respectively. The parameter η is evaluated using results from [23] for the attenuation length which is being taken as 190 and 175 g cm^{-2} respectively for P and Fe showers at 10 PeV. The atmospheric composition in the intermediate space between the shower front and the ground plane is assumed to contribute a thickness 0.15 g cm^{-2} per one meter traversal by the EAS. Thus for P and Fe initiated showers, $\eta \approx \frac{0.15}{190}$ and $\frac{0.15}{175}$ m^{-1} and we take $r_0 \sim 30.0$ m as used in KASCADE data analysis [12]. Taking $\Theta = 50^0$ and measuring $y_R \sim 211.0$ m from the Fig. 5.6, the model predicted value for x_C comes out to be about 14.33 m.

5.5.2 The gap length for different showers

It is clear that the GL arises from the influence of the atmospheric attenuation of electrons mainly in inclined showers. It is obvious that different types of secondary particles show dependence on the slant depth i.e. Θ or secΘ unequally.

But electron numbers or size in an EAS, at the observation level depends strongly on the high-energy particle production in the cascade by a primary particle in the upper part of the atmosphere [24, 25]. The hadronic interaction cross-section depends strongly on the nature of the EAS initiating particle and hence it would limit the electron size near the Earth surface. This electron content will eventually determine the elliptical shape of the LDD of electrons, and consequently, the magnitude of the GL in the ground. In the concerned energy range, the hadronic cross-section more or less increases logarithmically with energy [26] and therefore the considered primary energy might cause the shape of the LDD of electrons. We have used electron lateral density data obtained by our amended

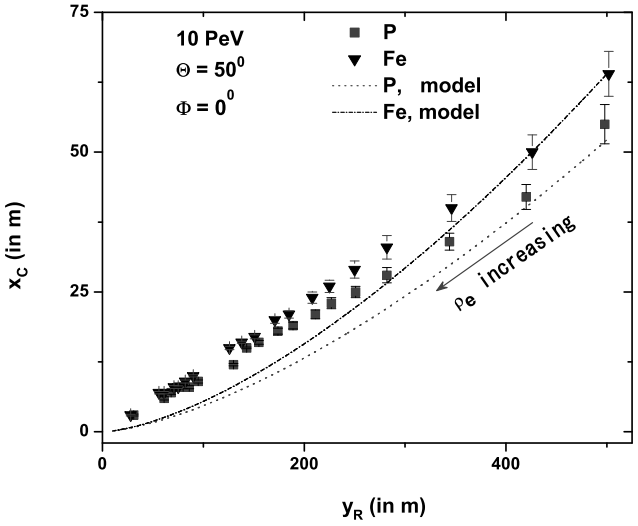

FIGURE 5.7: Variation of the GL (x_C) with y_R for the electron component. Predicted values for x_C are shown by the dotted and short dotted lines.

procedure to estimate the GL. The GL is evaluated corresponding to about seventeen equi-density data for electrons in the range $0.0003 - 0.5$ m^{-2}. In the Fig. 5.7, these lengths are shown with their respective y_R values for P and Fe initiated showers. The model predicted values are calculated using the KASCADE data for the attenuation length, in terms of which the expression for η is constructed out at 10 PeV. After substituting all the relevant parameters in the equation 5.21, we then have $x_C \cong 4.67 \times 10^{-}3.y_R^{1.5}$ m for P at $\Theta = 50^0$ while for Fe, it is $\cong 4.75 \times 10^{-}3.y_R^{1.53}$ m . It is clear from the figure, that the uncertainty in the estimation of GLs increases slightly with decreasing electron equi-densities. But, the percentage of error is relatively more for higher densities near the core which

does not look so visible in the figure. Discrimination among various primaries is clearly seen through the parameter x_C, corresponding to relatively smaller values of ρ_e. The dependencies of x_C on E and Θ are shown in Fig. 5.8 and Fig. 5.9 respectively. The values of x_C are greater, y_R being larger for 100 PeV compared to the curve for 10 PeV at each identical electron equi-density. The nature of variation of x_C with y_R for different Θ in the Fig. 5.8 is as per our expectation in accordance with the Fig. 5.1. Errors in these cases are found almost in the same sizes as those obtained in the Fig. 5.7.

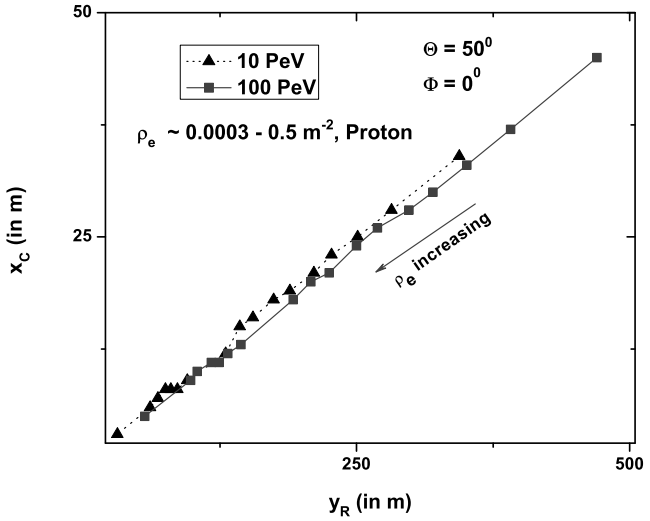

FIGURE 5.8: Variation of x_C with y_R for the electron densities for two energies, 10 and 100 PeV. The lines are only a guide for the eye.

5.5.3 Mass sensitivity of gap length and LAP

In the following, we have estimated x_C and LAP for different primaries, energies and zenith angles respectively and look for their sensitivity to the primary mass. It should be however mentioned, that, we have already got some indication about the mass dependence of the parameter x_C from the Fig. 5.7. Now we have to check the primary mass sensitivity of the LAP, previous studies [6, 7] investigated it using the NKG-type LDF for electrons.

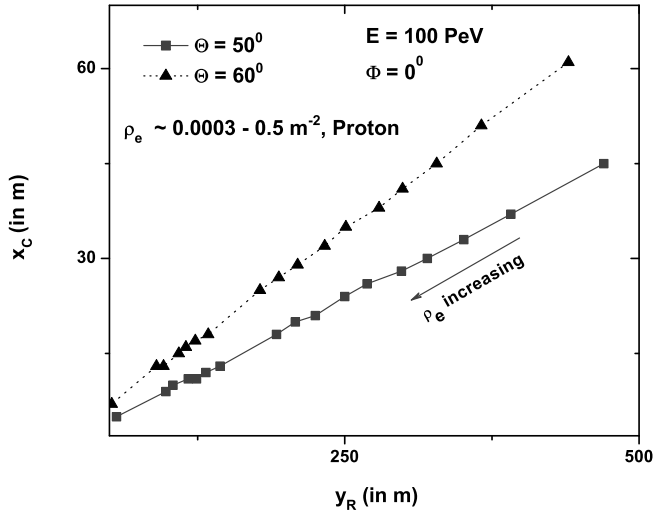

FIGURE 5.9: Variation between x_C and y_R at two zenith angles. The lines are only a guide for the eye.

5.5.3.1 Variation of gap length with shower size and zenith angle

5.5.3.2 Estimation of LAP and its mass sensitivity

We have studied the dependence of the x_C on the EAS observables N_e and Θ independently. A correlation between the mean x_C with N_e corresponding to $\Theta = 50^0$ and $\rho_e = 0.0003$ m^{-2} for p and Fe induced EASs, is set on view in Fig. 5.10 (**top**). We have used mean N_e for the above variation from a numerous number of showers induced at each primary energy. It is noticed that the x_C takes higher values for heavier nuclei compared to that of lighter ones, stating an important fact that equi-density ellipses of Fe initiated showers experience more stretching along the semi-major axis compared to p showers at a given ρ_e. Errors are of comparable sizes irrespective of p and Fe showers. In the Fig. 5.10 (**bottom**), we have studied the variation of x_C as a function of Θ for $\rho_e = 0.0003$ m^{-2} and $E = 100$ PeV respectively. The **bottom** figure is as per our expectation as described in the Sec.6.1. The simulated electron density data have been analyzed to obtain $s_{local}(r)$, using the SLDF and ELDF. The radial behaviour of the LAP has been investigated for p and Fe showers. The radial variation of the LAP corresponding to the SLDF and ELDF are shown in the Fig. 5.11 (**top**). Since the ELDF includes β_g, the variation of $s_{local}(r)$ is therefore performed at

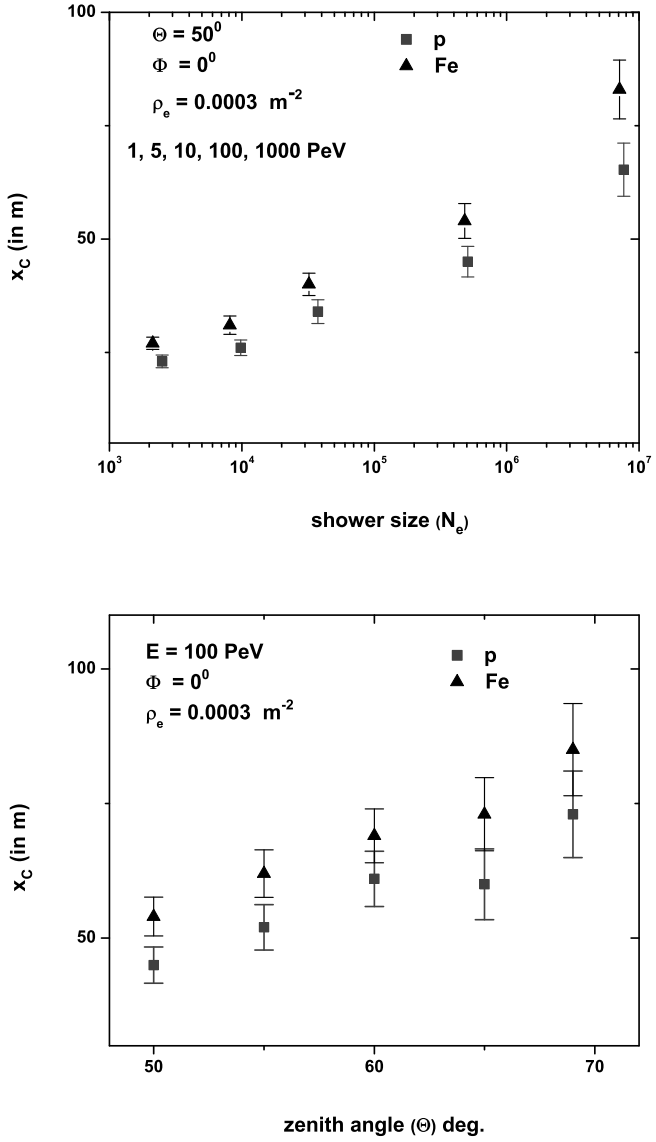

FIGURE 5.10: Mass sensitivity of the gap length parameter x_C from its variation with N_e (top). Same but with Θ (bottom).

two values of $< \beta_g >$; 0^0 and 45^0 respectively within a small angular bin, $\delta\beta = 2^0$ centered around their mean values. It is expected that the ELDF should vary with β_g according to the equation 5.30 while r_s is replaced by y_R. But, the above modification in the equation 5.30 has negligible effect on the LAP as revealed from the Fig. 5.11 (**top**). The Fig. 5.11 shows a difference between the curves of $s_{local}(r)$ versus r as obtained from the employment of SLDF and ELDF. Errors are not shown for the case of ELDF. The errors obtained in both the cases are quite large, possibly due to a smaller sample size of simulated showers at 10

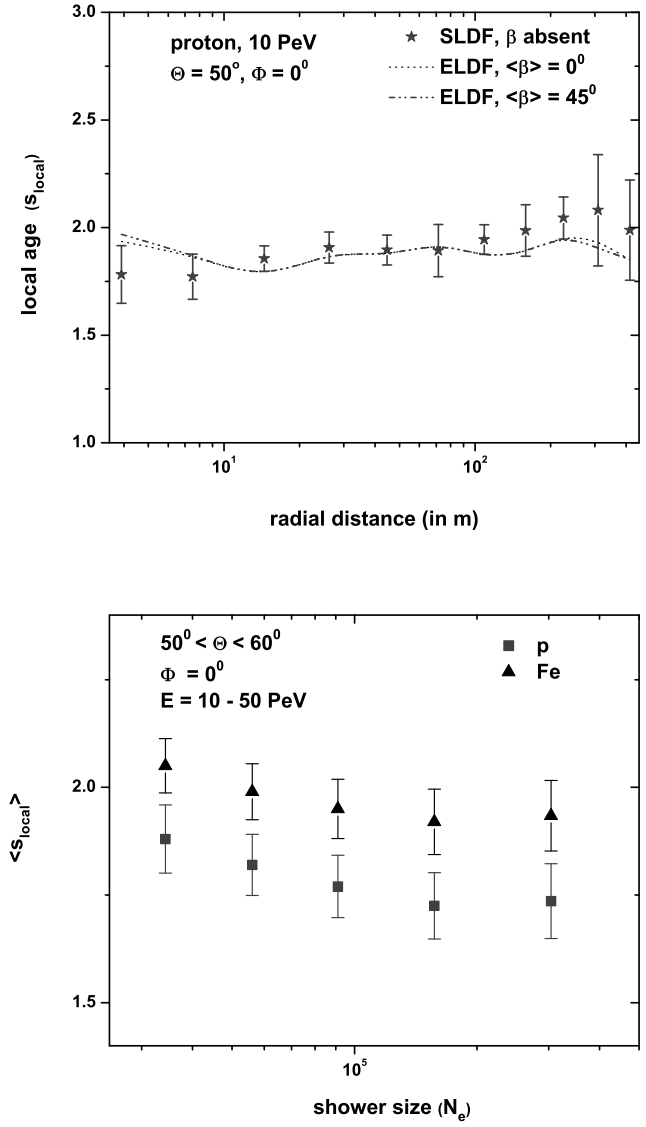

FIGURE 5.11: Variation of the LAP (estimated from the simulated data using SLDF (NKG) and ELDF) with radial distance at KASCADE level.

PeV.

Some recent studies [6, 7] have reported that the LAP first experiences some reduction in its value for smaller core distances, touches a minimum around 50 m, then starts increasing with core distance, reaches a maximum around 300 m and finally decreases monotonically. In those works, the radial dependence curve of LAP did not change its nature even for different energies of the primary [6]. A mean LAP was assigned to each shower, considering either the minimum value, or a mean value of all LAPs falling in the range $50 - 300$ m. Here, we have

obtained different radial variations for the LAP using SLDF and ELDF (see Fig. 11 - **top**) than earlier works. For the SLDF, the difference arises due to r_0, which is 30.0 m in this work, compared to 79.0 m in earlier works. On the other hand, the different r_0 and the inclusion of the attenuation effect with the GL into the ELDF are responsible for the mismatch. Owing to fluctuations from the Fig. 5.11 - **top**, we have chosen the radial range $25 - 75$ m in order to provide a uniform and consistent behavior to the LAP. Hence, a mean LAP is assigned to each EAS event from the average of all LAPs falling in that interval of r_g. A correlation between the mean LAP with N_e in the primary energy range, $3 \times 10^4 - 4.75 \times 10^5$ corresponding to a Θ range, $50^0 - 60^0$ for p and Fe induced EASs are given in Fig. 5.11 (**bottom**). The Fig 5.11 (bottom) clearly shows that the LAP still remains a very useful parameter for the measurement of CR mass composition.

5.6 Discussion

In this chapter, we have discussed the asymmetry of LDD of electrons using its polar variation in the ground plane for non-vertical showers. For inclined showers, with the EM component, the elliptic pattern of the LDD mainly arises from the different amount of atmosphere traversed by electrons around the EAS axis. It is noteworthy to mention that this chapter does not consider very highly inclined showers (generally $\geq 60^0$) for the purpose. For $\Theta \geq 60^0$, muons become a dominating component but suffering less against atmospheric attenuation, and therefore, might give smaller GL with greater uncertainty. The Fig. 10 (bottom) substantiates this fact that values of x_C for $\Theta > 60^0$ do not follow the trend which was seen initially for $\Theta \leq 60^0$. Uncertainties are also quite large due to reduction of electron numbers against strong attenuation of the EM component at these of Θ.

A modeling of the atmospheric attenuation effect on the LDD of electrons is made, and quantification of all new features obtained from it are the key areas of the work. Extraction of a new mass sensitive EAS observable x_C directly from the modeling of the attenuation effect, explores a new possibility of studying CR mass composition. Our investigation has used MC data generated by the *CORSIKA* code of version 6.970 for the purpose of implementation of the approach,

especially with regard to the authenticity of the gap in simulated data. Formulation of the GL between the EAS core and the center of equi-density ellipses resulted from a two-tier analytic method involving the interplay between two effects, the projection and the attenuation of EAS, to symmetric lateral electron densities. In doing so, a first order correction is allowed through the equation 5.17, applicable to arrays such as KASCADE, GRAPES-3 etc.

In EAS experiments, extraction of many useful information about the primary CRs, such as mass composition and the energy spectrum could only be possible from the characteristics of LDD of electrons, particularly at energies $\geq 10^{14}$ eV. Hence, the reconstruction of the LDD data in the observed plane by a more accurate LDF would only provide very precise estimation of the EAS observables to understand the nature of primary CRs. In this context, the ELDF is the appropriate to fulfill the purpose for the EAS experiments at sea level (large atmospheric depth is better for attenuation). Application of the accurate LDF (ELDF) has been substantiated in terms of the LAP, a very well studied EAS observable.

Asymmetry arises only from the influence of the Earth's magnetic field on the spatial distribution of muons with $\Theta > 60^0$ is another interesting research work which is in progress.

5.7 Conclusions

From the present analysis we conclude the following.

(1) An imprint of the attenuation effect on the EM component in an EAS is approximated through an elongation of equi-density pattern of simulated densities to ellipses. This causes a displacement of the center of these concentric ellipses to a new position. This work has quantified the displacement in terms of the GL parameter.

(2) The new parameter x_C is used in the work as a mathematical tool for describing the LDD of electrons more accurately in the ground plane. On the other hand, the parameter has shown its mass sensitivity for the measurement of CR mass composition. The variations of x_C with N_e and Θ separately have come up as potential studies to extract the nature of shower primary.

(3) From the experimental point of view, the accurate ELDF has been used to simulated electron densities to define the so-called LAP. A different radial variation of the modified LAP has been found. Moreover, a single mean shower age parameter to each EAS has been assigned to explore the mass sensitivity of the LAP. The mean LAP versus N_e plot is still being used to extract information about primary CRs.

Bibliography

[1] O Sima *et al. Nucl. Instrum. Methods in Phys. Res. A* **638** 147 (2011).

[2] A M Hillas, *Acta Phys. Acad. Sci.* **29(S3)** p.355 & p.533 (1970).

[3] H Rebel and O Sima, *Romanian Rep. Phys.* **59** 609 (2007).

[4] H Rebel *et al.*, *J. Phys. G:Nucl. Part. Phys.* **35** 085203 (2008).

[5] J N Capdevielle and J Gawin, *J. Phys. G: Nucl. Part. Phys.* **8** 1317 (1982).

[6] R K Dey, A Bhadra and J N Capdevielle, *J. Phys. G:Nucl. Part Phys.* **39** 085201 (2012).

[7] R K Dey and A Bhadra, *Astropart. Phys.*, **44** 68 (2013).

[8] A Cillis and S J Scieutto, *J. Phys. G:Nucl. Part. Phys.* **26** 309 (2000).

[9] M T Dova, M E Mancenido, A G Mariazzi, H Wahlberg, F Arqueros and D Garcia-Pinto, *Astropart. Phys.*, **31** 312 (2009).

[10] W D Apel *et al.*, *Astropart. Phys.*, **24** 467 (2006).

[11] S K Gupta *et al.*, *Nucl. Instrum. Methods,* A **540** 311 (2005).

[12] W D Apel *et al.*, *Astropart. Phys.*, **29** 317 (2008).

[13] S Dam, R K Dey and A Bhadra *Information Systems Design and Intelligent Applications* (India:Springer), **339** J K Mandal *et al.*, 1 (2015).

[14] K Greisen *Prog. in Cosmic Ray Phys. NH Publishing Co.*, Amsterdom (**V.III**) (1956).

[15] H S Snyder *Phy. Rev.*, **76** 1563 (1989).

[16] S Sanyal, B Ghosh, A Bhadra, A Mukherjee and N Chaudhuri, *Aust. J. Phys.*, **46** 589 (1993).

[17] D Heck, J Knapp, J N Capdevielle, G Schatz and T Thouw, *The CORSIKA Air Shower Simulation Program Forchungszantrum Karlsruhe Report*, **FZK6019** (1998).

[18] K Werner, F-Ming Liu and T Pierog *Phys. Rev. C*, **74** 044902 (2006).

[19] M Bleicher *et al.*, *J. Phys. G:Nucl. Part. Phys.* **25** 1859 (1999).

[20] W R Nelson, H Hiramaya and D W O Rogers *The EGS4 Code System Report* **SLAC 265** (1985).

[21] National Aeronautics and Space Administration (NASA) US Standard Atmosphere Technical Report **NASA - TM - X - 74335** (1976).

[22] M Kobal *Astropart. Phys.*, **15** 259 (2001).

[23] T Antoni *et al.*, *Astropart. Phys.*, **19** 703 (2003).

[24] N Nikolaev *Phys. Rev. D*, **48** 1904 (1993).

[25] R M Baltrusaitis *et al.*, *Phys. Rev. Lett.*, **52** 1380 (1984).

[26] R Ulrich, J Blumer, R Engel, F Schussler and M Unger *New J. Physics* **11** 065018 (2009).